Electronic Supplementary Information (ESI)

Insights into Plasmon Induced Keto-Enol Isomerization

Wei Zhang,[1,2†] Jie Kong,[1,2†] Huaxiang Chen,[3] Hongmei Zhao,[1] Tingting You,[3] Yuanyuan Guo,[1,2] Qianjin Guo,[1] Penggang Yin,[3*] Andong Xia[1,2*]

[1]Beijing National Laboratory for Molecular Sciences (BNLMS), Key Laboratory of Photochemistry, Institute of Chemistry, Chinese Academy of Sciences, Beijing 100190, China.

[2]University of Chinese Academy of Sciences, Beijing 100049, China.

[3]Key Laboratory of Bio-inspired Smart Interfacial Science and Technology of Ministry of Education, School of Chemistry, Beihang University, Beijing 100191,China.

[†]These authors contributed equally to this work.

Corresponding authors: andong@iccas.ac.cn; pgyin@buaa.edu.cn

Contents

Materials. Sodium oxalate, sodium citrate and $HAuCl_4$ were purchased from Sinopharm Chemical Reagent Co., Ltd. 2-mercapto-4(3H)-quinazolinone (MQ) as keto form was purchased from Sigma-Aldrich. The molecular structure of MQ is shown in Scheme S1a. Methanol (chromatographically pure) was purchased from Beijing Chemical Works. Ultrapure water (18.2 MΩ) from Milli-Q system was used throughout this study. All glassware was cleaned via aqua regia solution (HCl/HNO_3 = 3:1) and then washed by ultrapure water.

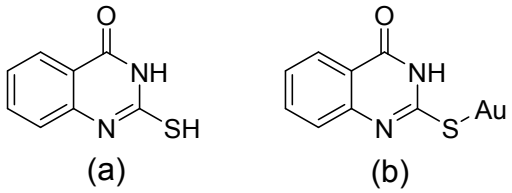

Scheme S1. The molecular structures of MQ as it received (a), and MQ on the gold nanoparticles surface (b).

Characterization. The UV-Vis absorption spectra was recorded with a U-3010 (Hitachi, Japan) spectrophotometer. Transmission electron microscopy (TEM) samples were dispersed in water and prepared by drop-casting a small amount of gold colloidal nanoparticles with or without MQ molecules onto 400 mesh copper grids. Fourier transform infrared spectroscopy (FT-IR) were performed on a Tensor-27 (Bruker, German) FT-IR spectrometer using KBr pellets.

S1. Gold Nanoparticles Synthesis and Characterization

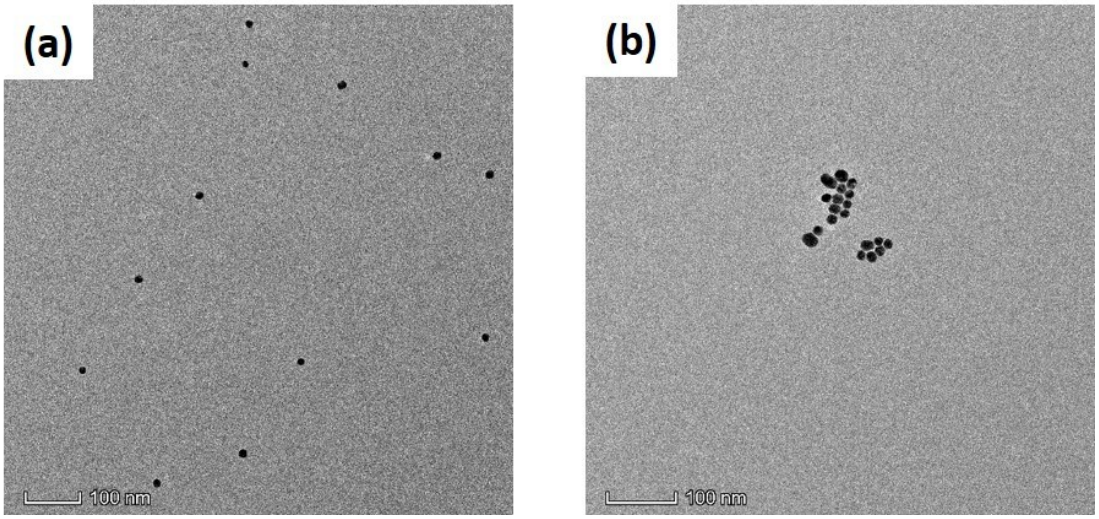

Fig. S1 TEM images of gold nanoparticles without (a) and with (b) MQ molecules (The molecular structure of MQ adsorbed on gold nanoparticles surface is shown in Scheme S1b).

15 nm gold nanoparticles were prepared according to citrate reduction method as described by Frens and Turkevich.[1,2] Briefly, 143 mL of aqueous $HAuCl_4$ (2.8×10^{-4} M) was prepared in a 200 mL three-necked round-bottomed flask and the solution brought to a boil, after which a solution of 38.8 mM

aqueous sodium citrate (7 mL) was added with continued boiling for 15 min. Then the color of boiling solution changed from yellow to faintly blue (nucleation) and then to a red wine color indicating the formation of gold colloid. The diameter of the prepared gold solution was 15 ± 2 nm according to TEM characterization (Fig. S1). The concentration of the gold nanoparticles solution was estimated to be 2.2 nM based on the diameter of gold nanoparticles (GNPs), the final volume of the stock solution, and the amount of starting materials. As the –SH functional group can be affected by pH, so the experimental sequence (MQ adding and pH adjusting, see Fig. S2) is not adjustable for this samples preparation process.

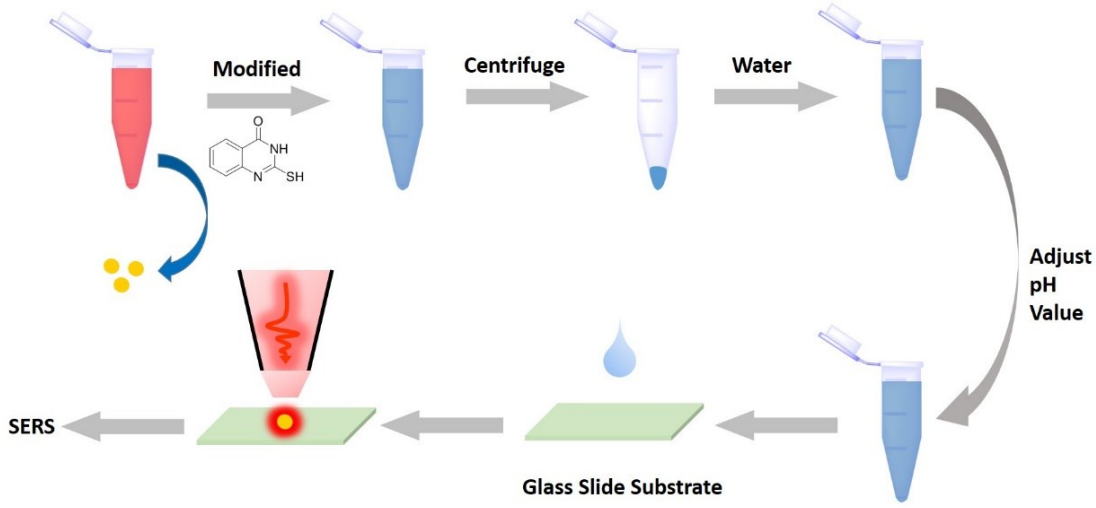

Fig. S2 SERS samples preparation process and measurements

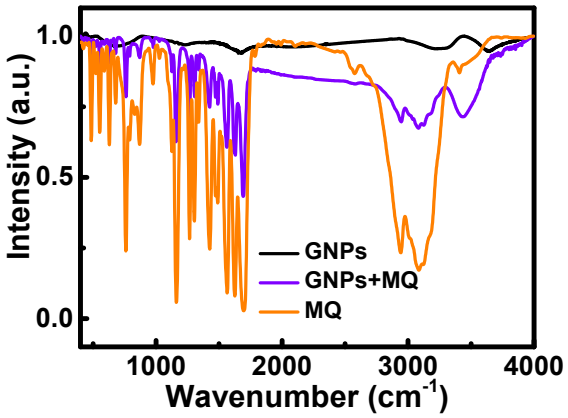

Fig. S3 The original FT-IR spectra of MQ, GNPs and MQ adsorbed onto GNPs.

S2. Theoretical Simulated Raman and SERS Spectra

As shown in Fig. S2, MQ methanol solution was added to gold colloid solution and incubated for more than 4 hours to ensure full equilibrium absorption of the MQ molecules onto GNPs surface.[3] The mixture was further centrifuged to remove the excess MQ molecules and washed by the mixture of Milli-Q water and methanol (v/v=2:1) for three times. Dilute HCl and NaOH solution were used to adjust the pH value of the mixture from 1 to 12, and then the droplets were transferred onto a clean glass slide to

obtain the SERS-active substrate. Raman spectroscopic measurements were performed by a LabRAM HR800 (Horiba Jobin Yvon) with an excited laser of 633 nm and 785 nm wavelengths.

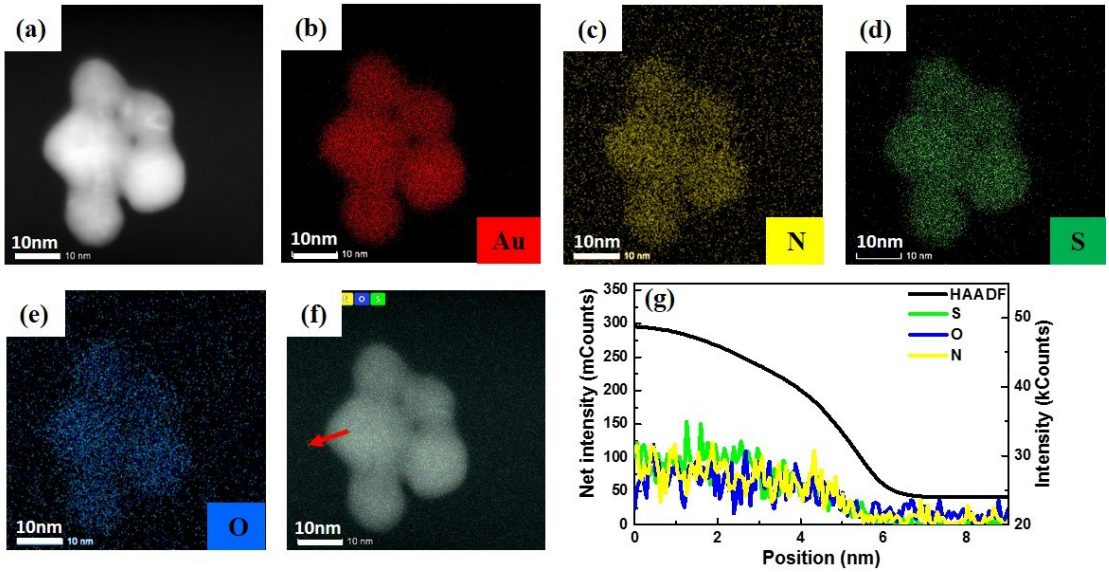

Fig. S4 HAADF-STEM image of GNPs after absorbing MQ molecules (a), elemental mapping and line scanning of MQ molecules adsorbing onto GNPs (b-g).

Fig. S4 shows scanning transmission electron microscopy energy dispersive X-ray spectroscopy (STEM-EDX) elemental mapping and high-angle annular dark-field (HAADF)-STEM image by using an FEI Talos 200S TEM system, and samples were degassed before the measurements.

Based on the density-functional theory (DFT), the geometry optimizations were performed using Gaussian 09 software package.[4] DFT calculations were carried out with the generalized gradient approximation (GGA) for exchange-correlation functionals, such as BLYP,[5,6] BP86,[5,7] and PW91PW91[8]. The hybrid exchange-correation functionals, such as B3PW91,[8,9] B3LYP,[10] PBE1PBE,[11] and B3P86[7,9] were also used. The basis sets for C, N, O, S and H atoms of MQ were 6-311++G (d, p), which include a polarization function of these five kinds of atoms and a diffuse function for C, N, O and S atoms. For the gold atoms, the basis set LANL2DZ was used to describe the valence electrons and the inner shell electrons, and the corresponding relativity effective core potentials, respectively.[12,13] For testing reliability of the theoretical calculations, the vibrational spectra of MQ were calculated via different functionals and compared with experimental spectra. It is found that the theoretical result at B3LYP/6-311++G(d,p) level is in good agreement with measured Raman spectrum of KF of MQ (Fig. S5a). In this case, all the corresponding calculations, including the Raman simulation, is also reasonably performed at B3LYP/6-311++G(d,p) level.

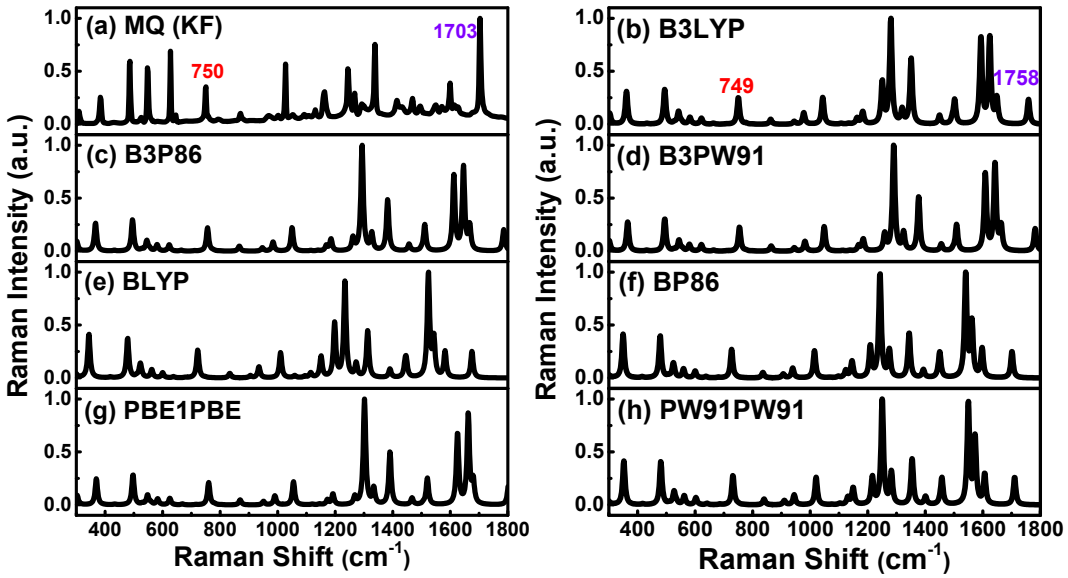

Fig. S5 (a) Normalized Raman spectrum of MQ (KF) with 633 nm laser excitation, the laser power is about 1.6mW (focused point on the sample is about 1 μm^2). (b)- (h) Calculated normal Raman spectra of MQ by using different functionals. An excitation wavelength of 633 nm and a line width of 10 cm^{-1} were used in the simulated spectra at 298.15 K.

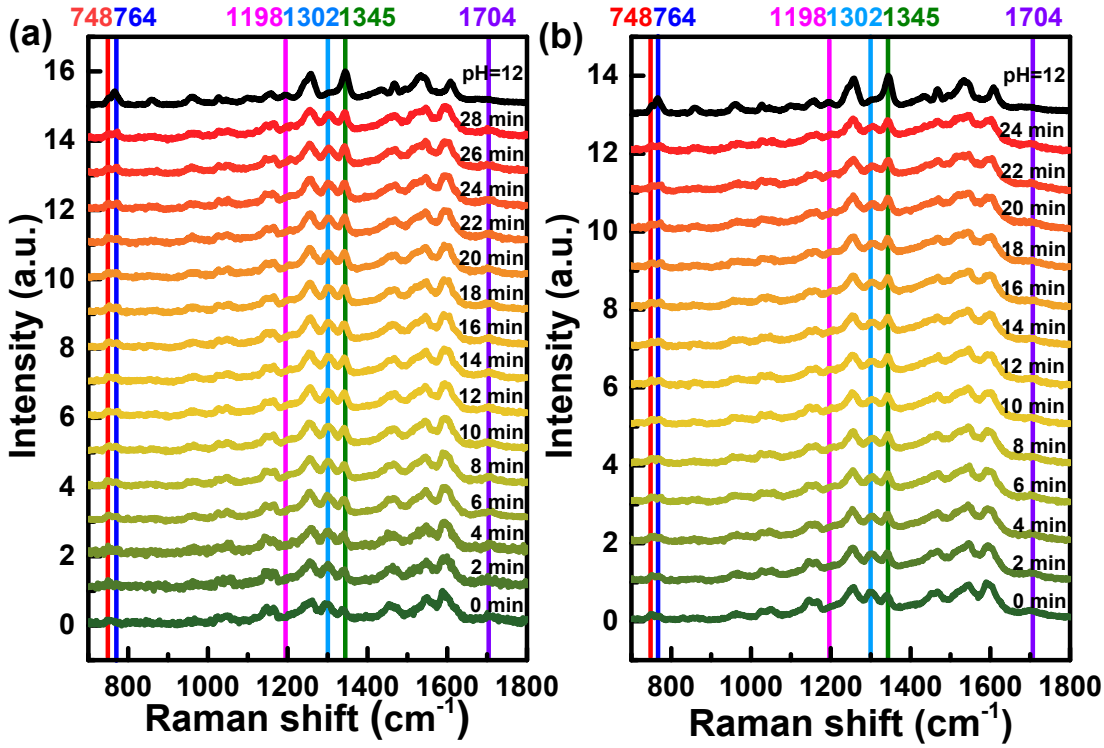

Fig. S6 Time-dependent SERS of MQ under excitation of 633 nm laser at pH 1(a) and pH 3(b). The SERS spectra under excitation of 633 nm at pH 12 are also displayed at the top of the Figures as comparison.

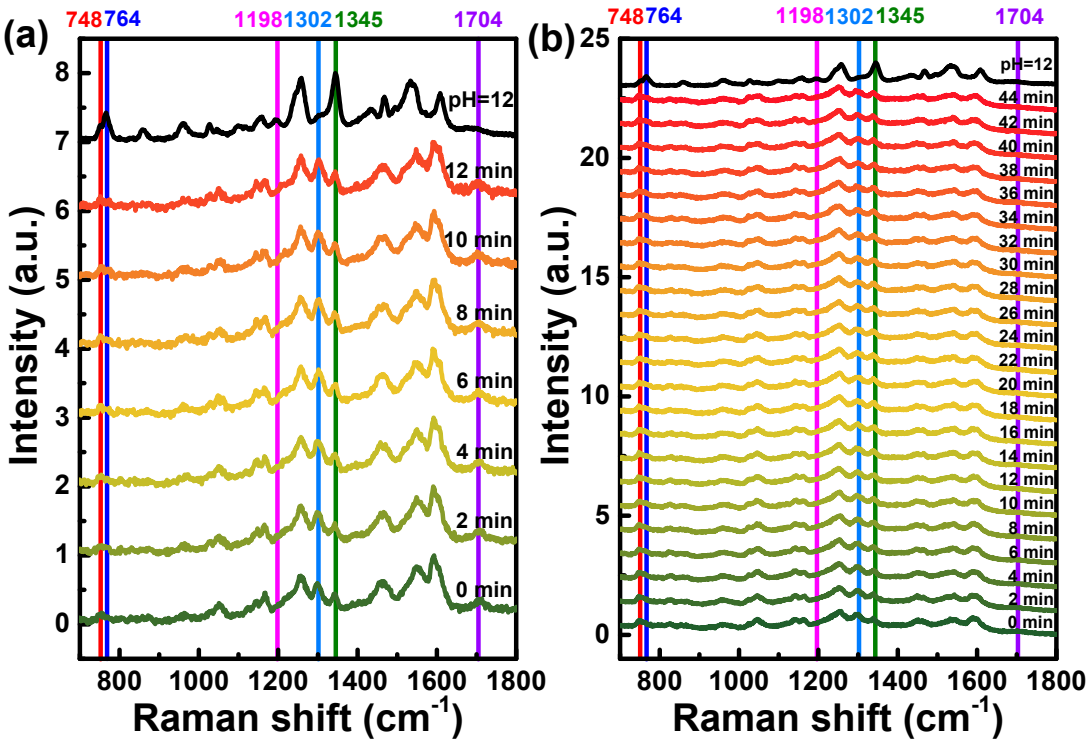

Fig. S7 Time-dependent SERS of MQ under excitation of 633 nm laser at pH 7(a) and under excitation of 785 nm wavelength laser at pH 5(b). The SERS spectra under excitation of 633 nm at pH 12 are also displayed at the top of the Figures as comparison.

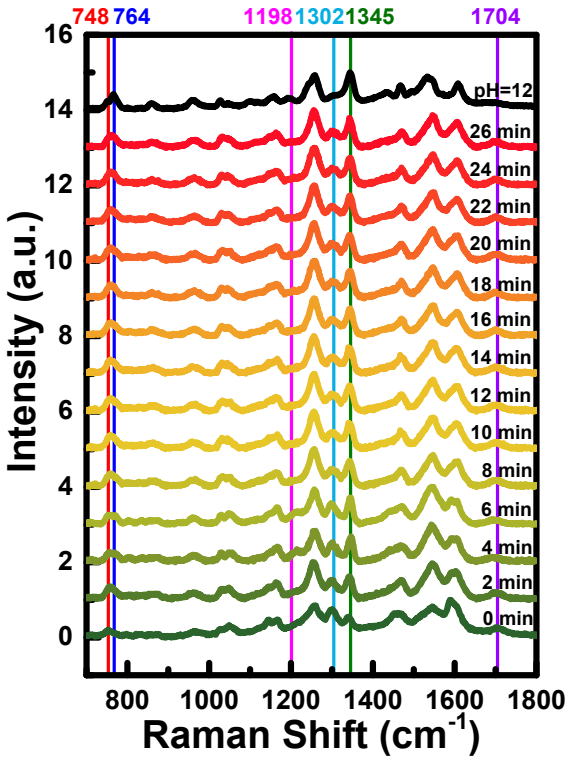

Fig. S8 Time-dependent SERS of MQ under excitation of 633 nm laser at pH 5 in the presence of sodium oxalate. The SERS spectra under excitation of 633 nm at pH 12 are also displayed at the top of the Figure as comparison. By introducing sodium oxalate (hole scavenger), the holes involved in the keto-enol

isomerization will be reduced as a result of the remolval of photoexcited holes (that is the holes captured by the sodium oxalate).

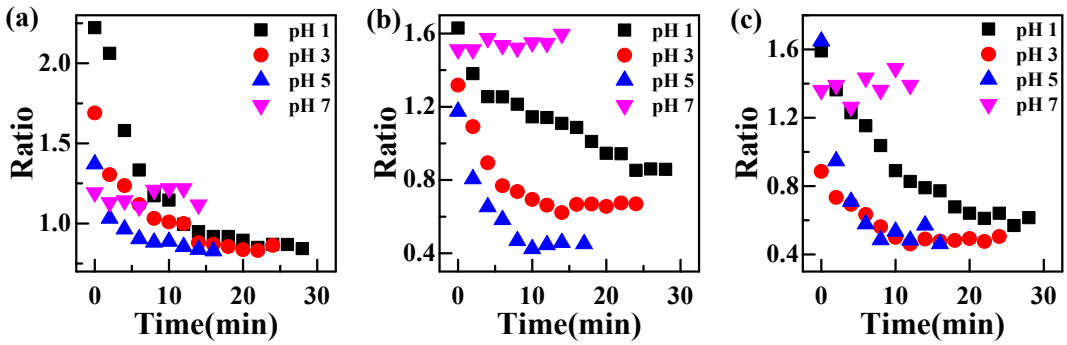

Fig. S9 The Raman peak intensity ratio of (a) KF (748 cm^{-1}) to EF (764 cm^{-1}), (b) KF (1302 cm^{-1}) to EF (1345 cm^{-1}) and (c) KF (1704 cm^{-1}) to EF (1198 cm^{-1}) as a function of reaction time under excitation of 633 nm laser.

S3. Chemical Calculations Details

The metallic cluster model was used to simulate the surface Raman spectra of MQ molecule on gold.[14] Thiophonol derivatives absorb onto gold surface, a strong Au-S chemical bond is formed between thiol group and gold surface after the cleavage of S-H bond. And the Au_5 cluster was used to allow MQ to absorb at bridge site on gold surface via the formation of Au-S bond. The gold cluster was ignored when we simulated the reaction transition states. It has been shown that the discrete electronic transion state in samll metal cluster can be adopted as an analogue of plasmon frequency and thus act as a model system to simulate the excitation of surface plasmon,[15] which has been widely used in many studies.[16-20] After the formation of chemical bond Au-S between GNPs and MQ, the energy level changes of MQ is negligibly small.[20] This is also evidenced by the UV-Vis spectra of MQ and MQ-GNPs complexes (see Fig. 4a), which shows almost identical absorption profiles of MQ with or without GNPs.[18]

Raman spectrum is used to measure the intensity of scattered light. And for a specific vibrational mode *i*, its Raman intensity I_i and Raman activity S_i are two different quantities. Raman intensity is depend on the excitation frequency of incident light as well as temperature, while Raman activity is an intrinsic property of molecular vibrational mode. The Gaussian output files show the Raman activity, and the conversion relationship between Raman activity and Raman intensity can be found in literatures:[21]

$$I_i = \frac{C(\nu_0 - \nu_i)^4 S_i}{\nu_i B_i}$$

$$B_i = 1 - e^{\left(-hc\nu_i / kT\right)}$$

where ν_i is vibrational frequency, and C is a suitable normalization factor for all peak intensities. And Multiwfn can used to finish this conversion. [22]

The geometries and energies of reactants, transition states and products were calculated via B3LYP[10]/6-311G++ (d,p) level. Bulk solvation effects were simulated via polarized continuum model (PCM) at the same level. All the calculation were performed by Gaussian 09 program package.[4] The density of states profiles were performed on Multiwfn program.[22]

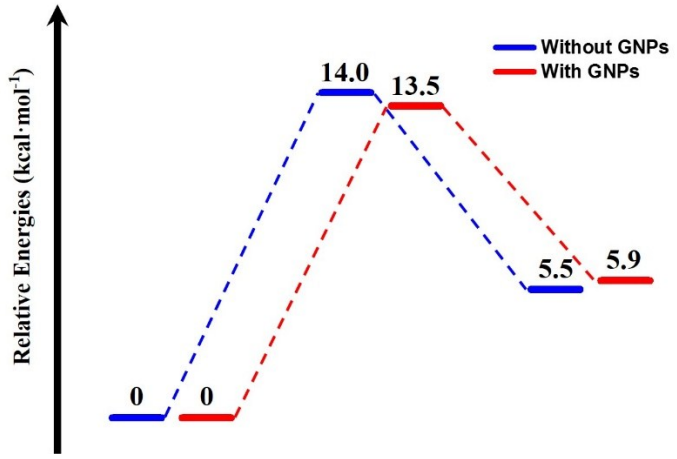

Fig. S10 Potential energy profiles for KF molecule isomerization. The energies (kcal·mol^{-1}) are obtained at the B3LYP/6-311++G(d,p) level. All energies given are relative to the reactant complex of KF with one water molecule.

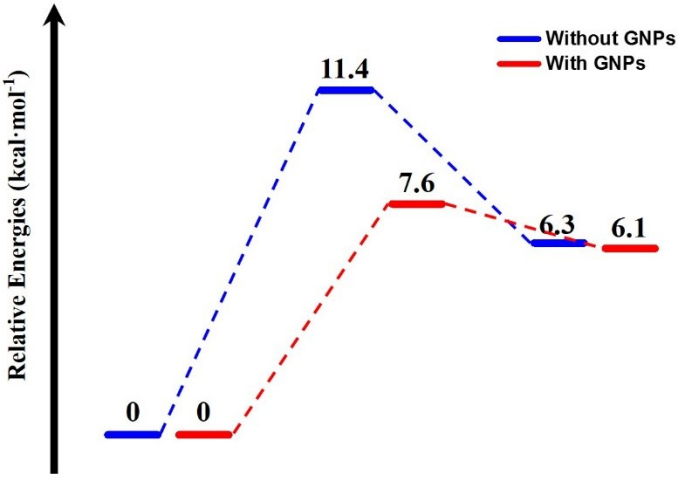

Fig. S11 Potential energy profiles for KF molecule isomerization. The energies (kcal·mol^{-1}) are obtained at the B3LYP/6-311++G(d,p) level. All energies given are relative to the reactant complex of KF with three water molecules.

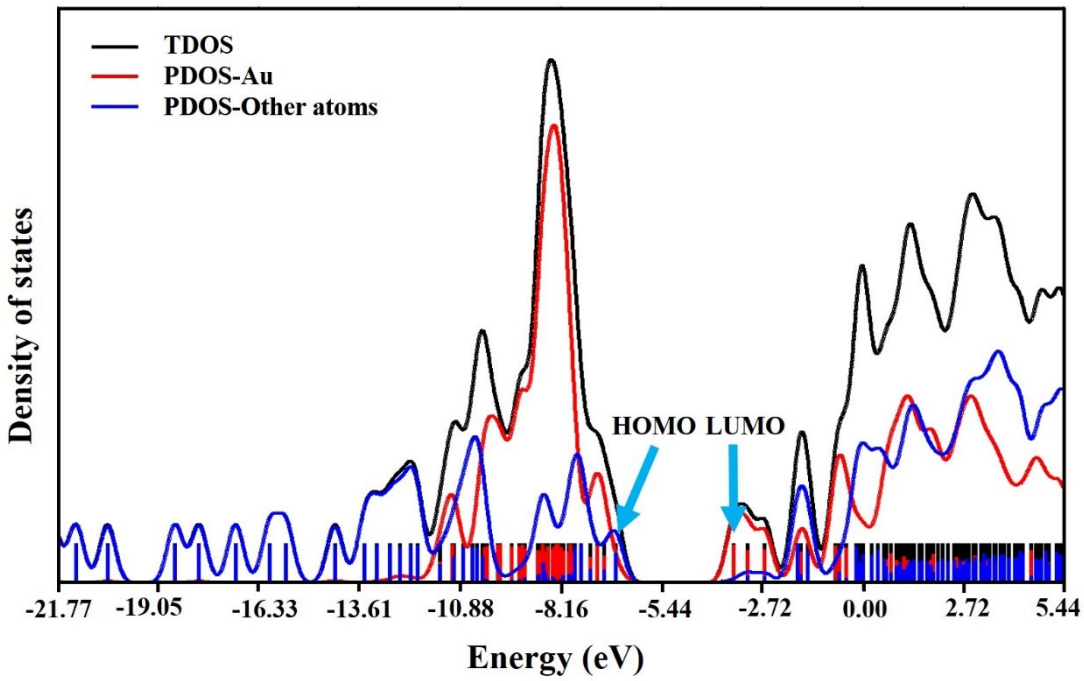

Fig. S12 Total density of states (TDOS) and partial density of states (PDOS) profiles for the complex of MQ-Au5. A Gaussian function with full width half height of 0.5eV was used to broadening molecular orbital energies to yield DOS curves.

Table S1. The optimized geometries of reactant, transition state and product systems at the level of B3LYP/6-311++G(d,p). Bond lengths are indicated in angstrom. Hydrogen, carbon, oxygen, nitrogen, sulfur atoms are denoted with white, gray, red, blue and yellow balls, respectively.

bond	reactant system	transition state system	product system
	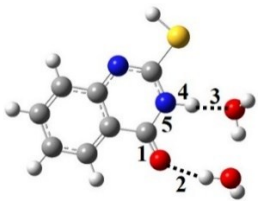	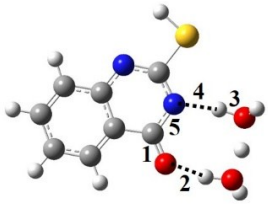	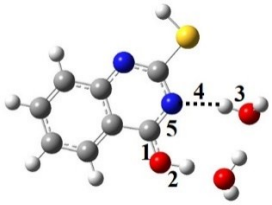
1	1.21932	1.24142	1.28962
2	1.94389	1.59695	1.03760
3	1.68450	1.01322	0.97532
4	1.05275	1.71453	2.04285
5	1.40075	1.37815	1.33361

Table S2. The energy barrier (kcal·mol^{-1}) of KF molecule isomerization catalyzed by GNPs assisted by different number of water molecule(s).

	without H_2O	one H_2O	two H_2O	three H_2O
energy barrier	44.7	13.5	6.7	7.6

S4. References

1. B. V. Enustun and J. Turkevich, *J. Am. Chem. Soc.*, 1963, **85**, 3317-3328.
2. G. Frens, *Nat. Phys. Sci.*, 1973, **241**, 20.
3. K.-Q. Lin, J. Yi, S. Hu, B.-J. Liu, J.-Y. Liu, X. Wang and B. Ren, *J. Phys. Chem. C*, 2016, **120**, 20806-20813.
4. G. W. T. M. J. Frisch, H. B. Schlegel, et al., *Gaussian 09, Revision E.01*; Gaussian, Inc.: Wallingford CT, 2013.
5. A. D. Becke, *Phys. Rev. A*, 1988, **38**, 3098-3100.
6. C. Lee, W. Yang and R. G. Parr, *Phys. Rev. B*, 1988, **37**, 785-789.
7. J. P. Perdew, *Phys. Rev. B*, 1986, **33**, 8822-8824.
8. J. P. Perdew, K. Burke and Y. Wang, *Phys. Rev. B*, 1996, **54**, 16533-16539.
9. A. D. Becke, *J. Chem. Phys.*, 1993, **98**, 5648-5652.
10. P. J. Stephens, F. J. Devlin, C. F. Chabalowski and M. J. Frisch, *J. Phys. Chem.*, 1994, **98**, 11623-11627.
11. J. P. Perdew, K. Burke and M. Ernzerhof, *Phys. Rev. Lett.*, 1996, **77**, 3865-3868.
12. P. J. Hay and W. R. Wadt, *J. Chem. Phys.*, 1985, **82**, 270-283.
13. P. J. Hay and W. R. Wadt, *J. Chem. Phys.*, 1985, **82**, 299-310.
14. D.-Y. Wu, X.-M. Liu, Y.-F. Huang, B. Ren, X. Xu and Z.-Q. Tian, *J. Phys. Chem. C*, 2009, **113**, 18212-18222.
15. S. M. Morton, D. W. Silverstein and L. Jensen, *Chem. Rev.*, 2011, **111**, 3962-3994.
16. T. Peng, J. Miao, Z. Gao, L. Zhang, Y. Gao, C. Fan and D. Li, *Small*, 2018, **14**, 1703510.
17. L. Jensen, C. M. Aikens and G. C. Schatz, *Chem. Soc. Rev.*, 2008, **37**, 1061-1073.
18. N. Kumar, S. Thomas, R. Rao, N. Maiti and R. J. Kshirsagar, *J. Phys. Chem. A*, 2019, **123**, 9770-9780.
19. L.-B. Zhao, M. Zhang, Y.-F. Huang, C. T. Williams, D.-Y. Wu, B. Ren and Z.-Q. Tian, *J. Phys. Chem. Lett.*, 2014, **5**, 1259-1266.
20. R. Wang, X.-R. Shen, M. Zhang, R. Devasenathipathy, R. Pang, D.-Y. Wu, J. Zhang, J. Ulstrup and Z.-Q. Tian, *J. Phys. Chem. C*, 2019, **123**, 23026-23036.
21. V. Krishnakumar, G. Keresztury, T. Sundius and R. Ramasamy, *J. Mol. Struct.*, 2004, **702**, 9-21.
22. T. Lu and F. Chen, *J. Comput. Chem.*, 2012, **33**, 580-592.